Supplementary Information to "Conformation-changing enzymes and macromolecular crowding"

Tomasz Skóra, Mihail N. Popescu, and Svyatoslav Kondrat

(Dated: March 11, 2021)

S1. BROWNIAN DYNAMICS SIMULATIONS

To perform Brownian dynamics (BD) simulations, we have used a customized version of the simulation package BD_BOX [1, 2]. The modification included the Lennard-Jones interactions between all types of "macromolecules", i.e., crowders and dumbbell enzymes, as well as the tailored bounding potentials involved in the flexible dumbbell enzyme model.

Brownian dynamics trajectories have been generated by using the second order Iniesta-de la Torre algorithm [2, 3]; within this algorithm, the position of ith bead at time t is

$$\boldsymbol{r}_i = \boldsymbol{r}_i^0 + \frac{1}{2}\frac{\Delta t}{k_B T}\sum_{j=1}^{N}\left(\boldsymbol{D}_{ij}^0\boldsymbol{F}_j^0 + \boldsymbol{D}_{ij}'\boldsymbol{F}_j'\right) + \boldsymbol{R}_i, \tag{S1}$$

where N is the number of beads, $\Delta t = t - t_0 > 0$ is the time step, $\boldsymbol{r}_i^0$ is the position of the ith bead at time t_0, k_B is the Boltzmann constant and T temperature. The (position-dependent) diffusion matrix $\boldsymbol{D}_{ij}^0$ (see below) and the force $\boldsymbol{F}_j^0$ acting on the jth bead are evaluated at time t_0, while $\boldsymbol{D}_{ij}'$ and $\boldsymbol{F}_j'$ are evaluated for beads in a configuration with the positions at an intermediate corrector step [3].

The $3N$ vector of random displacements, $\hat{\boldsymbol{R}} = \{\boldsymbol{R}_i\}$, is given by $\hat{\boldsymbol{R}} = \hat{\boldsymbol{B}}\hat{\boldsymbol{X}}$, where $\hat{\boldsymbol{X}}$ is a random Gaussian vector, and the matrix $\hat{\boldsymbol{B}} = \{\boldsymbol{B}_{ij}\}$ is a 'square root' of the diffusion tensor, *i.e.*,

$$\hat{\boldsymbol{D}} = \hat{\boldsymbol{B}}\hat{\boldsymbol{B}}^T \tag{S2}$$

where $\hat{\boldsymbol{D}} = \{\boldsymbol{D}_{ij}\}$. For the Iniesta-de la Torre algorithm, the diffusion matrix used in eq. (S2) is $(\hat{\boldsymbol{D}}^0 + \hat{\boldsymbol{D}}')/2$, so that the random forces satisfy

$$\langle \boldsymbol{R}_i \rangle = 0, \quad \langle \boldsymbol{R}_i \boldsymbol{R}_j^T \rangle = \Delta t \left(\boldsymbol{D}_{ij}^0 + \boldsymbol{D}_{ij}'\right). \tag{S3}$$

We used Cholesky decomposition to calculate $\hat{\boldsymbol{B}}$, as implemented in BD_BOX; it was performed each 100 steps to increase the performance, similarly as in ref. 4.

A. Bounding potentials

We consider a system of two beads (enzyme subunits) with the bead-bead interaction potential given by

$$U(\ell) = \frac{16\kappa}{(\ell_{\rm o} - \ell_{\rm c})^4} (\ell_{\rm c} - \ell)^2 (\ell_{\rm o} - \ell)^2, \tag{S4}$$

where $\ell_{\rm o}$ and $\ell_{\rm c} < \ell_{\rm o}$ correspond to the equilibrium separations in the 'open' and 'closed' states, respectively (Fig. 1 in the main text). Here, the characteristic energy set by the "spring constant" κ corresponds to the height of the energy barrier separating the two states. In order to model a system with all enzymes in the closed state due to binding a substrate, we take the single-well interaction potential $U_{\rm c}$

$$U_{\rm c}(\ell) = \frac{16\kappa}{(\ell_{\rm o} - \ell_{\rm c})^4} (\ell_{\rm c} - \ell)^2 g_{\rm c}(\ell), \tag{S5}$$

where

$$g_{\rm c}(\ell; \ell_{\rm c}, \ell_{\rm o}) = \begin{cases} (\ell_{\rm o} - \ell)^2, & \text{if} \quad \ell < \ell_{\rm c} \\ (\ell - 2\ell_{\rm c} + \ell_{\rm o})^2, & \text{if} \quad \ell > \ell_{\rm c}. \end{cases} \tag{S6}$$

It is easy to see that function $g_{\rm c}(\ell)$ is continuous with continuous first derivative, thus producing continuous forces. The choice above ensures a smooth matching with the double-well potential $U(\ell)$ (see main text) at the position of the minimum located at at ℓ_c.

B. Soft repulsion between pairs of particles (other than those belonging to the same dumbbell)

In all the numerical simulations we included a repulsive van der Waals interactions between any pairs of particles that did not belong to the same "enzyme", i.e., between crowder-crowder, crowder-enzyme, and enzyme-enzyme. This was computed as follows. Every particle was approximated by an ensemble of closed-packed spheres of radii $\sigma = 0.15\,\text{nm}$ ("atoms"); the interaction between the particles was then obtained *via* integration of the atom-atom Lennard-Jones repulsive potential (*i.e.* LJ12) over the volumes of two interacting particles. [5] If the closed-packed ensemble would lead to smooth spherical surfaces, the procedure renders for the interaction between two spheres of radii $a_{1,2} \gg \sigma$ separated

(center-to-center) by a distance r_{ij} the expression [5]

$$V_{LJ}^{rep}\left(r_{ij}\right)=\frac{\epsilon_{LJ}\pi^{2}}{315}\left(\frac{a_{i}a_{j}}{a_{i}+a_{j}}\right)\frac{\sigma^{6}}{\left[r_{ij}-\left(a_{i}+a_{j}\right)\right]^{7}}. \tag{S7}$$

However, this is often not the case and the surface of the closed pack ensemble provides an approximation as a rough surface, which can lead to significant decreases in the magnitude of the particle-particle interaction. [6, 7]. Following ref. 4, we account for this effect by introducing a roughness factor

$$A=\frac{r_{ij}-\left(a_{i}+a_{j}\right)}{r_{ij}-\left(a_{i}+a_{j}\right)+0.5\left(h_{i}+h_{j}\right)}, \tag{S8}$$

where $h_{i,j}$ characterizes the roughness of the particles i,j, respectively, which multiplies the right hand sides of eq. (S7) by A. The roughness may be estimated as the difference between the hydrodynamic and gyration radii [4]. For simplicity, here we simply assume the roughness to be of the order of the atom size, i.e., we take $h_i=\sigma(=0.15\,\mathrm{nm})$ for all i.

The aforementioned description of a large macromolecule as a sphere composed of small van der Waals atoms leads to an counter-intuitive picture of the macromolecule, in which the centers of van der Waals atoms are uniformly distributed over the volume of the whole sphere, and thus the outermost ones are partially not within the macromolecule. In order to ensure that all van der Waals atoms fit inside the macromolecules, for the sake of computing interactions, hydrodynamic radii are decremented by a value equal to the radius of van der Waals atom (we took $\sigma=0.15\,\mathrm{nm}$)

$$a_i\mapsto a_i^{*}=a_i-\sigma. \tag{S9}$$

Radii a_i^{*} were also considered as a bead radius and used for computing occupied volumes.

In all the numerical simulations we used a lower and an upper cut-off for the distance between pairs of particles, as follows. For particles with surface-to-surface separation below 0.1 nm, the repulsive force is assumed constant (and equal to the value at the 0.1 nm separation). This is done in order to avoid numerical problems due to very large forces (note the strong divergence of eq. (S7) at $r_{ij}=a_i+a_j$). The upper cutoff for computing (numerically) van der Waals interactions was set to $r_{ij}^{(max)}=15\,\mathrm{nm}$, i.e., we set $V_{LJ}^{rep}(r_{ij}\geq r_{ij}^{(max)})=0$.

Finally, we note that for all the pairs of particles for which V_{LJ}^{rep} is relevant we have used $\epsilon_{LJ}=0.37\,\mathrm{kcal\,mol^{-1}}$. This choice follows ref. 4, which successfully reproduced the *in vivo* diffusion coefficient of the green fluorescent protein (GFP) in a complex model of cytoplasm by using the ϵ_{LJ} value above.

C. Hydrodynamic interactions

To account for hydrodynamic interactions, we employed the generalized Rotne-Prager-Yamakawa tensor [8–10], which reads (a_i is the bead's hydrodynamic radius, r_{ij} the center-to-center separation between the i'th and j'th beads, η is viscosity, and $\boldsymbol{I}$ is the unit tensor):

$$\boldsymbol{D}_{ii} = \frac{k_B T}{6\pi\eta a_i}\boldsymbol{I}; \tag{S10a}$$

$$\boldsymbol{D}_{ij}(r_{ij}) = \frac{k_B T}{8\pi\eta r_{ij}}\left[\left(1+\frac{a_i^2+a_j^2}{3r_{ij}^2}\right)\boldsymbol{I} + \left(1-\frac{a_i^2+a_j^2}{r_{ij}^2}\right)\frac{\boldsymbol{r}_{ij}\boldsymbol{r}_{ij}^T}{r_{ij}^2}\right] \tag{S10b}$$

for $r_{ij} > a_i + a_j$;

$$\boldsymbol{D}_{ij}(r_{ij}) = \frac{k_B T}{8\pi\eta r_{ij}}\left[\frac{16r_{ij}^3(a_j+a_j) - [(a_i-a_j)^2+3r_{ij}^2]^2}{32r_{ij}^3}\boldsymbol{I} + \frac{3[(a_i-a_j)^2-r_{ij}^2]^2}{32r_{ij}^3}\frac{\boldsymbol{r}_{ij}\boldsymbol{r}_{ij}^T}{r_{ij}^2}\right] \tag{S10c}$$

for $a_{ij}^M - a_{ij}^m < r_{ij} < a_i + a_j$, where a_{ij}^M is the largest and a_{ij}^m the smallest of a_i and a_j; and

$$\boldsymbol{D}_{ij} = \frac{k_B T}{6\pi\eta a_{ij}^M}\boldsymbol{I}, \tag{S10d}$$

for $r_{ij} < a_{ij}^M - a_{ij}^m$.

D. Simulation parameters

The box size was 25 nm × 25 nm × 25 nm and periodic boundary conditions were applied in all three directions. In order to account for the long-range character of the hydrodynamic interactions, we used the Ewald summation [11], as implemented in the BD_BOX [1, 2]. The parameter controlling the convergence of the Ewald summation was $\sqrt{\pi}$ (default value in BD_BOX). The maximal magnitude of both real and reciprocal lattice vectors was 2. For computational efficiency, the diffusion tensor was updated once per 100 steps [4, 12] (each update causes the Cholesky decomposition).

In all the numerical simulations the temperature was set to $T = 298.15\,\mathrm{K}$ (room temperature) and the viscosity of the medium (need for the computation of the hydrodynamic interactions) was set to the value $\eta = 1.02\,\mathrm{cP}$, corresponding to water.

The time step Δt (eq. (S1)) was set to 0.5 ps; a BD simulation runs for at least 4×10^10 iterations steps, i.e., a total time of at least 10 µs.

E. Trajectory analysis

We used FREUD library [13] to calculate mean square displacement MSD $= \langle |\boldsymbol{r}(t) - \boldsymbol{r}(0)|^2 \rangle$

$$\mathrm{MSD}(m\Delta t) = \frac{1}{N_{\mathrm{traj}}} \sum_{i=1}^{N_{\mathrm{traj}}} \frac{1}{N_{\mathrm{steps}} - m} \sum_{k=0}^{N_{\mathrm{steps}}-m-1} \{\boldsymbol{r}_i\,[(k+m)\Delta t] - \boldsymbol{r}_i\,[k\Delta t]\}^2, \tag{S11}$$

where N_{traj} is the number of trajectories and N_{steps} the total number of steps. The shift Δt in trajectory analysis was 5 ns.

The time-dependent relative apparent diffusion coefficient is:

$$\frac{D(t)}{D_0} = \frac{\mathrm{MSD}(t)}{6D_0 t}, \tag{S12}$$

where D_0 is diffusion coefficient in infinite dilution. For a spherical particle, D_0 is given by the Stokes-Einstein equation.

The long-time diffusion coefficients D_l have been obtained by fitting to a constant the numerical results for $\frac{D(t)}{D_0}$ in a time window around $t = 5\,\mu$s.

Uncertainty of the simulation results due to sampling error was estimated by dividing the simulations into 5 subsets and treating them as independent 'measurements'.

S2. BEAD-BEAD AVERAGE SEPARATION AND THE PROBABILITIES OF THE OPEN AND CLOSED STATES IN THE CASE [S] = 0

In the case of single, isolated enzyme, the probability density $\mathcal{P}(l)$ of finding the enzyme subunits separated by a distance ℓ is governed by the Boltzmann distribution:

$$\mathcal{P}\left(l\right) dl = \frac{l^2 \exp\left(-\frac{U}{k_B T}\right) dl}{\int_0^\infty l^2 \exp\left(-\frac{U}{k_B T}\right) dl}. \tag{S13}$$

It is convenient to restrict the continuous phase space to a two state model by classifying enzymes with $l \geq \ell_{\rm m} = (\ell_{\rm o} + \ell_{\rm c})/2$ as open and the remaining ones as closed. Then, the probabilities p_o and p_c of finding the enzyme in the open and in the closed state, respectively, are given by

$$p_{\rm o} = \frac{\int_{\ell_{\rm m}}^\infty l^2 \exp\left(-\frac{U}{k_B T}\right) dl}{\int_0^\infty l^2 \exp\left(-\frac{U}{k_B T}\right) dl}. \tag{S14}$$

$$p_{\rm c} = \frac{\int_0^{\ell_{\rm m}} l^2 \exp\left(-\frac{U}{k_B T}\right) dl}{\int_0^\infty l^2 \exp\left(-\frac{U}{k_B T}\right) dl} = 1 - p_{\rm o}. \tag{S15}$$

For a single enzyme with $\kappa = 6.8\, k_B T$, $\ell_{\rm o} = 2.5a$, and $\ell_{\rm c} = 1.1a$ we obtained $p_{\rm o} \approx 0.83$.

In the case of crowded systems, the corresponding $\mathcal{P}(l)$ functions are computed from the BD simulations, specifically from the separation histograms.

S3. OCCUPIED VOLUMES

We computed volume occupied by a single dumbbell in any state (table S1) as the average value of the volume $V(l)$:

$$\langle V \rangle = \frac{\int_0^\infty V(l)\, l^2 \exp\left(-\frac{U}{k_B T}\right) dl}{\int_0^\infty l^2 \exp\left(-\frac{U}{k_B T}\right) dl}. \tag{S16}$$

where (see the main text Fig. 1a for the overlapping geometry)

$$V(l) = \begin{cases} 2 \times \frac{4}{3}\pi a^3, & l \geq 2a\,, \\ \frac{4}{3}\pi a^3 + l\pi a^2 - \frac{1}{12}\pi l^3, & l < 2a \end{cases}. \tag{S17}$$

TABLE S1. Occupied volumes of single enzymes with the binding potentials U_c and U, corresponding to $[S] \to \infty$ and $[S] = 0$, respectively (eqs. (S16) and (S17)).

potential	$\langle V \rangle$ / V_{bead}
U_c	1.747
U	1.959

S4. MONTE CARLO SIMULATIONS FOR OCCUPIED AND EXCLUDED VOLUMES

To compute the occupied and excluded volumes for systems from our BD simulations for a given tracer (*cf.* Tables S2 and S3), we used a Monte Carlo method as follows. First, several snapshots of the BD simulation are selected [12]. Then, the following procedure is employed to each of the snapshots:

1. The positions of the particles are loaded from the selected BD snapshot;
2. The *tracer* is thrown into the system at a randomly generated position;
3. Iff the *tracer* overlaps with any other of the particles in the box, a counter variable n is incremented by one;
4. The tracer is removed from the system and steps 2-3 are repeated N times;
5. After N such trials, the value $\frac{n}{N}$ is taken as an estimate of the excluded volume fraction $\phi_{\mathrm{ex}}^{\mathrm{tracer}}$.

To compute the average excluded volume for a given *system*, the above simulations have been performed with $N = 10^4$ and 8 snapshots (at $2.0, 3.0, 4.0, 5.0, 6.0, 7.0, 8.0,$ and $9.5\,\mu\mathrm{s}$), for 5 distinct repeats of the simulation.

Occupied volume was computed in a similar manner, the only difference being that the insertion attempts use a point particle.

S5. SCALED PARTICLE THEORY FOR TWO-STATE ENZYMES UNDER CROWDING

For hard convex particles, the scaled-particle theory predicts that the change ΔF in the free energy between the two states (denoted as 'open' and 'closed', respectively) of a shape-changing object in the presence of crowders is given by [14, 15]

$$\Delta F(\phi_{\rm occ}) = \Delta F_0 + k_{\rm B}T \sum_{k=1}^{3} \frac{g_k(\phi_{\rm occ})}{(1-\phi_{\rm occ})^k} \,. \tag{S18a}$$

Here, ΔF_0 denotes the change in the free energy between the same two states in the absence of crowders, and the dimensionless functions g_k are given by

$$g_1(\phi_{\rm occ}) = \Delta H \langle A \rangle + \Delta A \langle H \rangle + \Delta V \langle 1 \rangle, \tag{S18b}$$

$$g_2(\phi_{\rm occ}) = \frac{1}{2} \left[\Delta H^2 \langle A \rangle^2 + 2 \Delta V \langle H \rangle \langle A \rangle \right], \tag{S18c}$$

$$g_3(\phi_{\rm occ}) = \frac{1}{3} \Delta V \langle H^2 \rangle \langle A \rangle^2 \,. \tag{S18d}$$

ΔV, ΔA, ΔH and ΔH^2 denote the differences in the volume, surface area, Kihara parameter (half of the projection of a particle onto any axis, averaged over all orientations of the particle) and its square ($\Delta H^2 = H_o^2 - H_c^2 \neq (\Delta H)^2$), respectively, of the particle in the open and closed states. They are independent of $\phi_{\rm occ}$; these parameters can be computed, if the shape of the particle in the two states is known, or — as in the case of experiments with active enzymes, if the shapes are not *a priori* known — they represent fitting parameters for experimental data. The bracketed terms refer to the following weighted sum of the corresponding observable for crowders (with G as a generic notation for such an observable):

$$\langle G \rangle = \frac{1}{\mathcal{V}} \sum_{k=1}^{M} N_k G_k, \tag{S19}$$

where $\mathcal{V}$ is the volume of the system, M is the number of different types of crowders, and N_k the number of crowders of type k (the total number of crowders being $N = \sum_{k=1}^{M} N_k$). (Note that $\langle H^2 \rangle = (1/\mathcal{V}) \sum_{k=1}^{M} N_k H_k^2 \neq \langle H \rangle^2$, while $\langle 1 \rangle = N/\mathcal{V}$, *i.e.*, it gives the number density of the crowders.) They capture the full dependence of the functions g_k on $\phi_{\rm occ}$, and they can be calculated *a priori*, since in general the number of crowders and their type (shape) are known.

To illustrate these ideas, we use the case of a particle with one type of crowders, spherical beads of radius a_c. In this case, eq. (S18) reduces to

$$\Delta F = \Delta F_0 + k_{\mathrm{B}}T \sum_{k=1}^{3} h_k \left(\frac{\phi_{\mathrm{occ}}}{1-\phi_{\mathrm{occ}}} \right)^k , \tag{S20a}$$

where

$$h_1 = \frac{3\Delta H}{a_c} + \frac{3\Delta A}{4\pi a_c^2} + \frac{3\Delta V}{4\pi a_c^3}, \tag{S20b}$$

$$h_2 = \frac{9\Delta H^2}{2a_c^2} + \frac{9\Delta V}{4\pi a_c^3}, \tag{S20c}$$

and

$$h_3 = \frac{9\Delta V}{4\pi a_c^3}. \tag{S20d}$$

For an enzyme with two-state kinetics, eq. (4) of the main text combined with eq. (S20)(a) can be used to fit experimental data on the activity of the enzyme in crowded environments to extract the parameters $h_{1,2,3}$ and $p_{\mathrm{o}}(0)$. (Note that, in order to do so, at least four experimental points must be available; obviously, for a robust, reliable fit, in practice much more many points are required.) Then, from eq. (S20)(b-d) one can interpret these parameters in terms of microscopic properties (ΔV, ΔA, ΔH, ΔH^2) of the shape-changes of the enzyme.

If additional information is available about the particle, a fitting procedure as discussed above can be strongly constrained by additional relations between the fitting parameters. For example, consider a spherocylindrical particle, of radius a and lengths ℓ_{o} and ℓ_{c} in the 'open' and 'closed' states, respectively. In this case, eq. (S20)(b-d) further simplify to

$$h_1 = \frac{3\Delta\ell}{4a_c} \left(1 + \frac{2a}{a_c} + \frac{a^2}{a_c^2} \right), \tag{S21a}$$

$$h_2 = \frac{9a\Delta\ell}{4a_c^2} \left(1 + \frac{a}{a_c} \right) + \frac{9\Delta\ell^2}{32a_c^2}, \tag{S21b}$$

and

$$h_3 = \frac{9a^2\Delta\ell}{4a_c^3}, \tag{S21c}$$

where $\Delta\ell = \ell_{\mathrm{o}} - \ell_{\mathrm{c}}$ and $\Delta\ell^2 = \ell_{\mathrm{o}}^2 - \ell_{\mathrm{c}}^2$. The number of fitting parameters is now reduced to two ($\Delta\ell$ and $\Delta\ell^2$), consistent with the fact that for this case h_1 and h_3 differ only through a constant (and given) proportionality factor.

A. Application to the fluctuating-dumbbell enzyme

We now discuss the use of the scaled particle theory in the case of a fluctuating-dumbbell enzyme in order to predict the dependence of the activity on $\phi_{\rm occ}$. This can be done by approximating (in order to satisfy the convex-shape requirement) the shape of the enzyme with that of a spherocylinder with lengths $\ell_{\rm o}$ and $\ell_{\rm c}$ in the open and closed states, respectively.

Since in our simulations we had both spherical crowders and enzymes, the number of different crowders in eq. (S19) is $M = 3$ (spherical beads, enzymes in the open states, and enzymes in the closed states). The shapes of the crowders, as well as that of the enzyme (spherocylinder particle), being specified, the functions g_k in eq. (S18) can be determined once the number densities of the three types of crowders are provided. Although the number of enzyme crowders that are in the open and closed states, respectively, is not known *a priori*, one can estimate $p_{\rm o} = N_{\rm o}/N_{\rm e}$ ($N_{\rm e} = N_{\rm o} + N_{\rm c}$ is the total number of enzymes) via an iterative procedure as follows. One starts with ΔF calculated at the initial value of $p_{\rm o}$, taken at no crowding, that is, $p_{\rm o}(0)$. Then, eq. (1) of the main text is used to obtain a new estimate for $p_{\rm o}$; this is then plugged into eq. (S18) to recalculate ΔF, and so on. (We have checked against the simulations that this procedure converges and provides consistent approximations for $p_{\rm o}$.)

The results are shown in Fig. S1 for two cases discussed in the main text, when crowding is due to spherical particles and enzymes (we recall that in the latter case about 5.2 % of the volume is occupied by the enzymes; in the former case about 2.5 % of the volume is occupied by the spherical particles). Clearly, the scaled-particle theory provides a good estimate of the activity reduction. The deviations from the BD simulations are likely because we approximated the enzyme as a spherocylinder. For comparison, we also show the SPT results in the case when crowding is solely due to spherical particles. These results overestimate the activity reduction only slightly when the majority of the crowders are spherical particles. Larger deviations are observed when crowding is mainly due to the enzymes, which is likely because of inaccuracies in determining the occupied volume fractions.

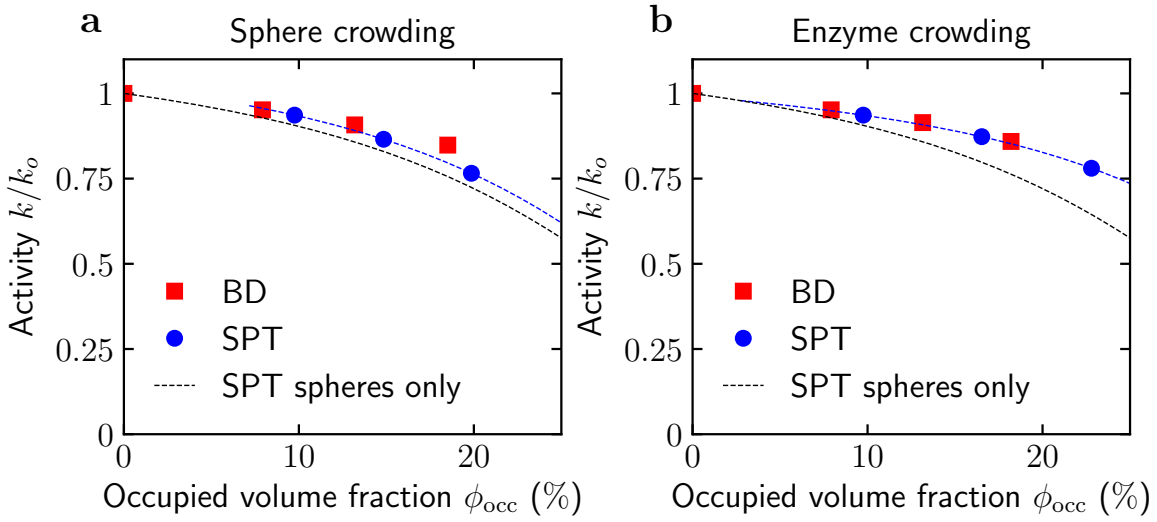

FIG. S1. **Brownian dynamics (BD) simulations** *vs.* **scaled-particle theory (SPT).** (**a**) Results for systems where crowding is due to spherical particles. All simulation systems contained 100 enzymes to gather enough statistics, which amounts to about 5.2 % in terms of the occupied volume fraction. In the SPT, the enzymes are approximated as spherocylinders. The black dash line shows the results when the crowding is solely due to spherical particles. (**b**) The same as (a) but for crowding created by enzymes. All these systems contained 100 spherical particles, which is about 2.5 % in terms of the occupied volume fraction.

S6. SUPPLEMENTARY FIGURES AND TABLES

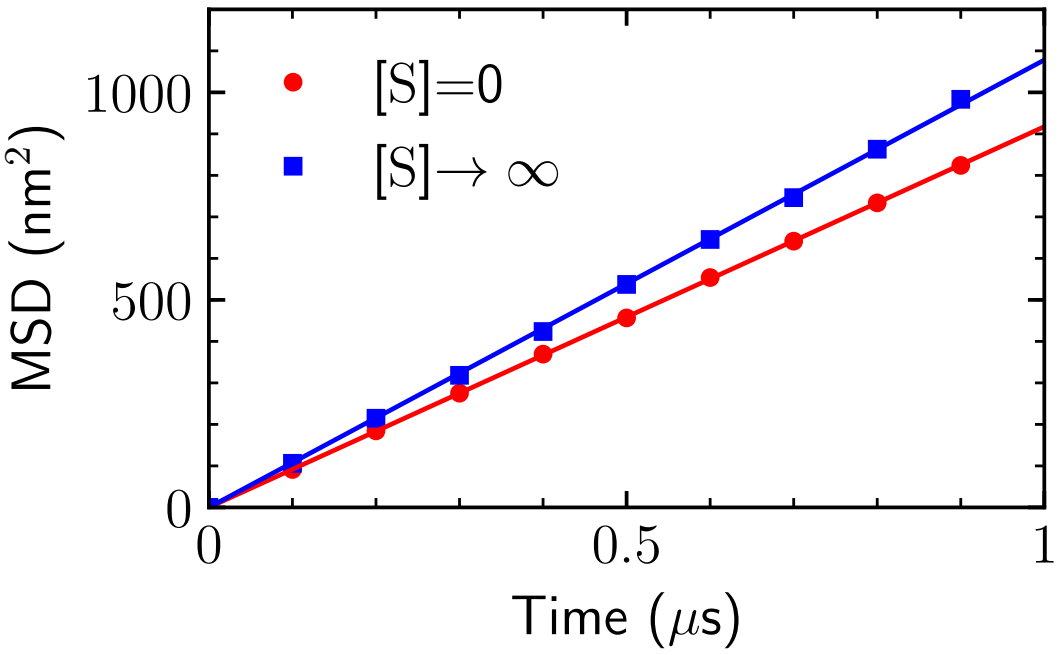

FIG. S2. **Mean-square displacement for a single enzyme with and without a substrate.** The MSDs result from 4000 independent simulations. The diffusion coefficients have been extracted by fitting the MSD(t) data with the linear function $f(t) = 6Dt$. The resulting diffusion coefficients are $D_0 \approx 153\,\mathrm{nm^2\,\mu s^{-1}}$ and $D_0^{(s)} \approx 180\,\mathrm{nm^2\,\mu s^{-1}}$ for the systems with [S] = 0 and [S] $\to \infty$, respectively.

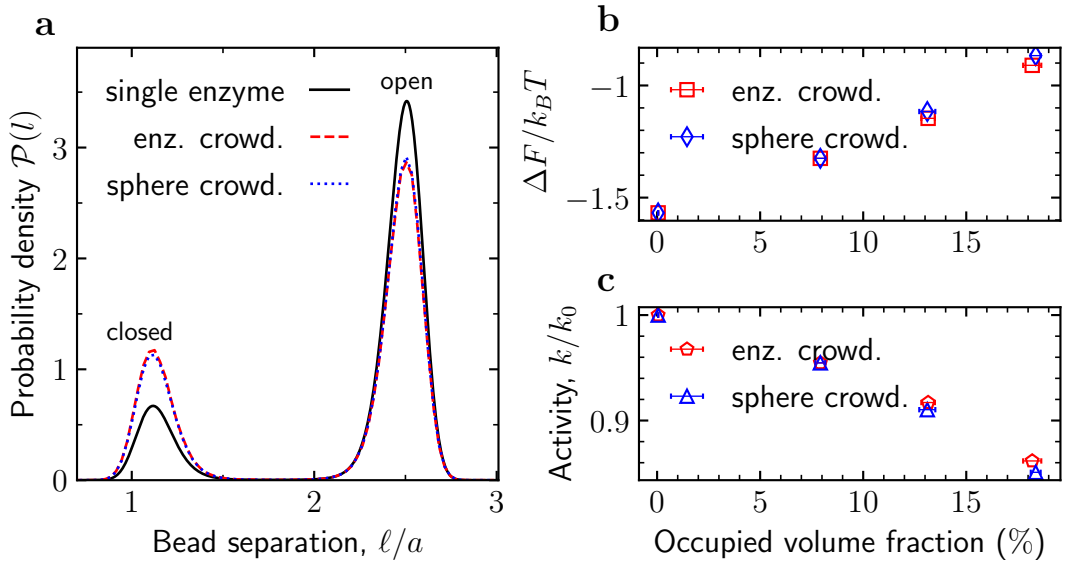

FIG. S3. **Differences in enzyme conformation and activity in systems with different composition.** (**a**) Probability density $\mathcal{P}(\ell)$ of finding the enzyme subunits separated by a distance ℓ in systems composed of 100 enzymes and 492 passive tracers (sphere crowding, blue dashed line), and 300 enzymes and 100 tracers (enzyme crowding, red dashed line). The occupied volume fraction ϕ_{occ} is the same for the two systems. (**b**) Free energy of opening ΔF as a function of the occupied volume fraction ϕ_{occ}. The squares (diamonds) denote the values of ΔF obtained from the BD simulations according to eq. (**??**) (main text) for systems with enzyme (sphere) crowding. (**c**) Reduction of the enzyme's catalytic activity, k/k_0, as a function of the occupied volume fraction ϕ_{occ}. The pentagons (triangles) denote the values obtained from the BD simulations (eq. (3)) for systems with enzyme (sphere) crowding.

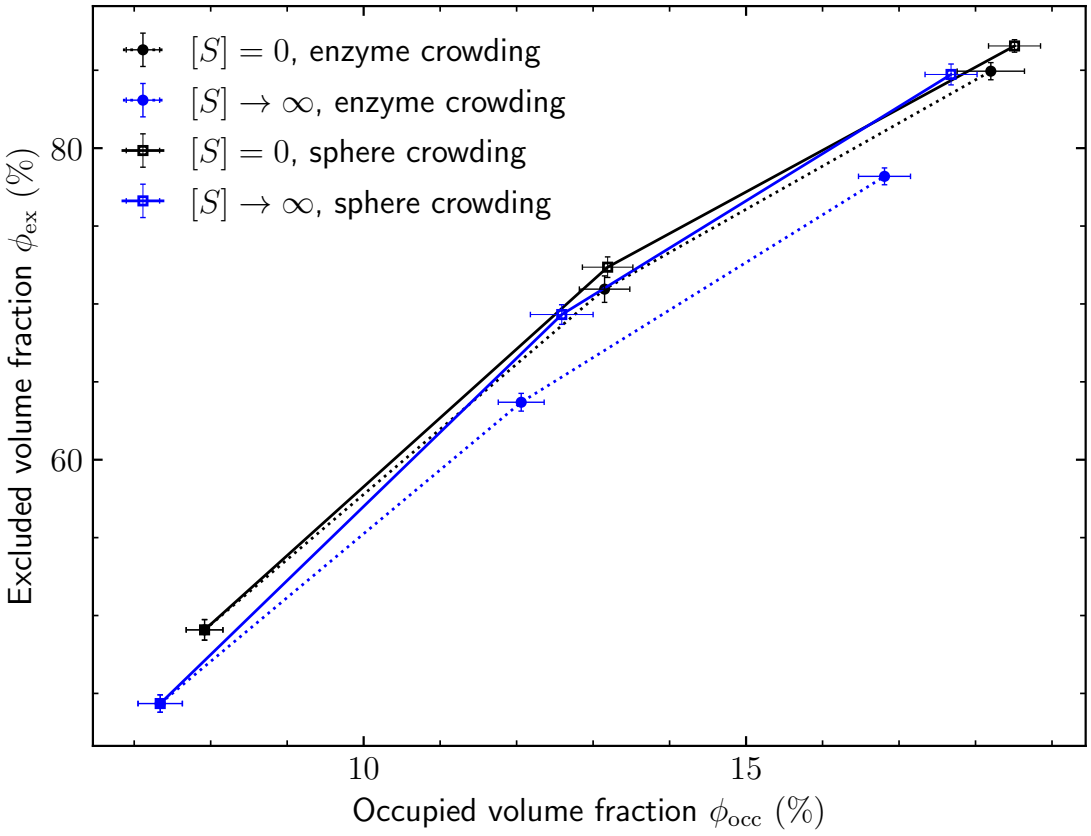

FIG. S4. **Excluded *vs* occupied volume fractions for the simulated mixtures.** The volume fractions have been computed with Monte-Carlo approach (Section S3). For the values see Tables S2 and S3).

TABLE S2. Occupied (ϕ_{occ}) and excluded ($\phi_{\mathrm{ex}}^{\mathrm{tracer}}$) volume fractions from Monte Carlo tracer insertion simulations for sphere crowding. The excluded volumes are shown for spherical crowders ($\phi_{\mathrm{ex}}^{\mathrm{sphere}}$) and for enzymes in the open and closed states ($\phi_{\mathrm{ex}}^{\mathrm{open}}$ and $\phi_{\mathrm{ex}}^{\mathrm{closed}}$, resepectively).

Sphere crowding					
N_{enz}	N_{tr}	ϕ_{occ} (%)	$\phi_{\mathrm{ex}}^{\mathrm{sphere}}$ (%)	$\phi_{\mathrm{ex}}^{\mathrm{closed}}$ (%)	$\phi_{\mathrm{ex}}^{\mathrm{open}}$ (%)
			[S] = 0		
100	100	7.92 ± 0.24	49.08 ± 0.66	61.27 ± 0.88	70.68 ± 0.67
100	296	13.19 ± 0.33	72.36 ± 0.66	84.16 ± 0.45	90.70 ± 0.50
100	492	18.51 ± 0.34	86.56 ± 0.40	94.42 ± 0.37	97.73 ± 0.15
			[S] $\to \infty$		
100	100	7.34 ± 0.29	44.35 ± 0.56	56.06 ± 0.45	65.72 ± 0.89
100	296	12.59 ± 0.41	69.32 ± 0.63	81.32 ± 0.46	88.71 ± 0.45
100	492	17.68 ± 0.34	84.73 ± 0.67	93.66 ± 0.68	97.16 ± 0.46

TABLE S3. Occupied (ϕ_{occ}) and excluded ($\phi_{\mathrm{ex}}^{\mathrm{tracer}}$) volume fractions from Monte Carlo tracer insertion simulations for enzyme crowding. The excluded volumes are shown for spherical crowders ($\phi_{\mathrm{ex}}^{\mathrm{sphere}}$) and for enzymes in the open and closed states ($\phi_{\mathrm{ex}}^{\mathrm{open}}$ and $\phi_{\mathrm{ex}}^{\mathrm{closed}}$, resepectively).

Enzyme crowding					
N_{enz}	N_{tr}	ϕ_{occ} (%)	$\phi_{\mathrm{ex}}^{\mathrm{sphere}}$ (%)	$\phi_{\mathrm{ex}}^{\mathrm{closed}}$ (%)	$\phi_{\mathrm{ex}}^{\mathrm{open}}$ (%)
0	100	2.68	19.98 ± 0.45	27.10 ± 0.44	33.63 ± 0.66
			[S] = 0		
100	100	7.92 ± 0.24	49.08 ± 0.66	61.27 ± 0.88	70.68 ± 0.67
200	100	13.15 ± 0.33	70.95 ± 0.85	82.84 ± 0.80	89.42 ± 0.50
300	100	18.20 ± 0.44	84.94 ± 0.55	93.16 ± 0.42	96.86 ± 0.35
			[S] $\to \infty$		
100	100	7.34 ± 0.29	44.35 ± 0.56	56.06 ± 0.45	65.72 ± 0.89
200	100	12.06 ± 0.30	63.69 ± 0.57	75.75 ± 1.10	84.44 ± 0.68
300	100	16.81 ± 0.34	78.19 ± 0.54	88.74 ± 0.40	94.09 ± 0.26

[1] BDBOX, \url{https://www.fuw.edu.pl/˜mdlugosz/downloads.html}.

[2] M. Długosz, P. Zieliński, and J. Trylska, Brownian dynamics simulations on CPU and GPU with BD_BOX, J. Comput. Chem. **32**, 2734 (2011).

[3] A. Iniesta and J. de la Torre, A second-order algorithm for the simulation of the Brownian dynamics of macromolecular models, J. Chem. Phys. **92**, 2015 (1990).

[4] T. Ando and J. Skolnick, Crowding and hydrodynamic interactions likely dominate in vivo macromolecular motion, Proc. Natl. Acad. Sci. U. S. A. **107**, 18457 (2010).

[5] D. Henderson, D.-M. Duh, X. Chu, and D. Wasan, An expression for the dispersion force between colloidal particles, J. Colloid Interface Sci. **185**, 265 (1997).

[6] J. Czarnecki and T. D˜bros, Attenuation of the van der Waals Attraction Energy in the Particle/Semi-Infinite Medium System Due to the Roughness of the Particle Surface, J. Colloid Interface Sci. **78**, 25 (1980).

[7] C. M. Roth, B. L. Neal, and A. M. Lenhoff, Van der Waals interactions involving proteins, Biophys. J. **70**, 977 (1996).

[8] J. Rotne and S. Prager, Variational treatment of hydrodynamic interaction in polymers, J. Chem. Phys. **50**, 4831 (1969).

[9] H. Yamakawa, Transport properties of polymer chains in dilute solution: hydrodynamic interaction, J. Chem. Phys. **53**, 436 (1970).

[10] P. J. Zuk, E. Wajnryb, K. A. Mizerski, and P. Szymczak, Rotne–Prager–Yamakawa approximation for different-sized particles in application to macromolecular bead models, J. Fluid Mech. **741**, R5 (2014).

[11] E. R. Smith, I. K. Snook, and W. Van Megen, Hydrodynamic interactions in Brownian dynamics: I. Periodic boundary conditions for computer simulations, Phys. A Stat. Mech. its Appl. **143**, 441 (1987).

[12] T. Skóra, F. Vaghefikia, J. Fitter, and S. Kondrat, Macromolecular Crowding: How Shape and Interactions Affect Diffusion, J. Phys. Chem. B **124**, 7537 (2020).

[13] V. Ramasubramani, B. D. Dice, E. S. Harper, M. P. Spellings, J. A. Anderson, and S. C. Glotzer, freud: A software suite for high throughput analysis of particle simulation data, Comput. Phys. Commun. **254**, 107275 (2020), arXiv:1906.06317.

[14] J. L. Lebowitz, E. Helfand, and E. Praestgaard, Scaled particle theory of fluid mixtures, J. Chem. Phys. **43**, 774 (1965).

[15] A. P. Minton, Molecular crowding: analysis of effects of high concentrations of inert cosolutes on biochemical equilibria and rates in terms of volume exclusion, Meth. Enzymol. **295**, 127 (1998).